BIOCHEMISTRY
including biophysical chemistry & molecular biology

Article

pubs.acs.org/biochemistry

YC-1 Binding to the β Subunit of Soluble Guanylyl Cyclase Overcomes Allosteric Inhibition by the α Subunit

Rahul Purohit,[†] Bradley G. Fritz,[†] Juliana The,[†] Aaron Issaian,[†] Andrzej Weichsel,[†] Cynthia L. David,[‡] Eric Campbell,[∥] Andrew C. Hausrath,[†] Leida Rassouli-Taylor,[§] Elsa D. Garcin,[§] Matthew J. Gage,[∥] and William R. Montfort*,[†]

[†]Department of Chemistry and Biochemistry, The University of Arizona, Tucson, Arizona 85721, United States
[‡]Center for Toxicology, College of Pharmacy, The University of Arizona, Tucson, Arizona 85721, United States
[§]Department of Chemistry and Biochemistry, University of Maryland, Baltimore County, Baltimore, Maryland 21250, United States
[∥]Department of Chemistry and Biochemistry, Northern Arizona University, Flagstaff, Arizona 86011, United States

ABSTRACT: Soluble guanylate cyclase (sGC) is a heterodimeric heme protein and the primary nitric oxide receptor. NO binding stimulates cyclase activity, leading to regulation of cardiovascular physiology and making sGC an attractive target for drug discovery. YC-1 and related compounds stimulate sGC both independently and synergistically with NO and CO binding; however, where the compounds bind and how they work remain unknown. Using linked equilibrium binding measurements, surface plasmon resonance, and domain truncations in *Manduca sexta* and bovine sGC, we demonstrate that YC-1 binds near or directly to the heme-containing domain of the β subunit. In the absence of CO, YC-1 binds with a K_d of 9−21 μM, depending on the construct. In the presence of CO, these values decrease to 0.6−1.1 μM. Pfizer compound 25 bound ∼10-fold weaker than YC-1 in the absence of CO, whereas compound BAY 41-2272 bound particularly tightly in the presence of CO (K_d = 30−90 nM). Additionally, we found that CO binds much more weakly to heterodimeric sGC proteins (K_d = 50−100 μM) than to the isolated heme domain (K_d = 0.2 μM for *Manduca* β H-NOX/PAS). YC-1 greatly enhanced binding of CO to heterodimeric sGC, as expected (K_d ∼ 1 μM). These data indicate the α subunit induces a heme pocket conformation with a lower affinity for CO and NO. YC-1 family compounds bind near the heme domain, overcoming the α subunit effect and inducing a heme pocket conformation with high affinity. We propose this high-affinity conformation is required for the full-length protein to achieve high catalytic activity.

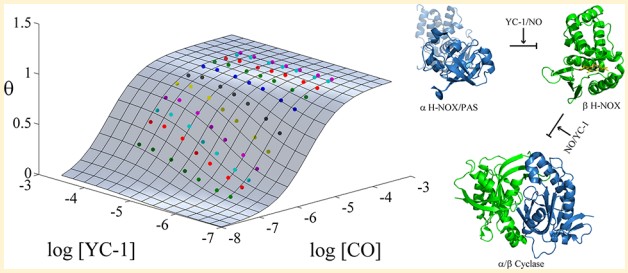

Nitric oxide (NO) regulates a phenomenal array of physiological processes, including blood pressure homeostasis, wound healing, memory formation, sexual response, and the fighting of infectious disease.[1] Impairment in NO signaling can lead to hypertension and atherosclerosis and contribute to heart attack and stroke.[2,3] NO is produced by a class of enzymes called nitric oxide synthases (NOSs) through the oxidation of L-arginine to L-citrulline.[4,5] The primary receptor for NO is soluble guanylyl/guanylate cyclase (sGC), a heterodimeric heme protein of ∼150 kDa that responds to binding of NO to heme through enhanced cyclase activity, producing cGMP and a signaling cascade. Treatment of cardiovascular disease by stimulating the nitric oxide pathway has long been a treatment goal, beginning more than 150 years ago with the administration of amyl nitrite[6] and nitroglycerin[7] to relieve symptoms of angina pectoris, although the mode of action of these compounds (release of NO) was not discovered until many years later. More recently, sGC, the NO receptor, has been heavily targeted for drug discovery.

sGC is composed of two homologous subunits, α and β. Multiple isoforms of each subunit have been identified; however, the most common isoform is the α_1/β_1 heterodimer (reviewed in ref 8). Each sGC subunit consists of four domains, an N-terminal heme-nitric oxide oxygen (H-NOX) domain[9] (also called a SONO domain[10]), a central Per-Arnt-Sim (PAS) domain,[11] a coiled-coil domain, and a C-terminal catalytic cyclase domain.[12] There is a single heme moiety in the heterodimer, associated with the β_1 H-NOX domain. The equivalent domain in the α_1 subunit has lost the ability to bind heme but appears to have retained an overall H-NOX-like fold and is therefore commonly termed the α_1 H-NOX domain. During signaling, the binding of NO to heme in the β_1 subunit leads to the formation of a pentacoordinated Fe−NO complex with proximal histidine bond breakage.[13−15] The structural change due to this event is transferred to the cyclase domain, which in turn enhances cGMP production. How this structural change is translated to increased catalytic activity is poorly understood. Moreover, elusive structural details for sGC have

Received: November 8, 2013
Revised: December 12, 2013
Published: December 16, 2013

hampered the understanding of allosteric regulation in the protein. Structures of individual sGC domains such as the β_1 coiled-coil homodimer,[16] the α_1 PAS domain,[17] and the α_1/β_1 heterodimeric cyclase domain[18] have recently been determined. Insight into the H-NOX and PAS domains comes from the structures of prokaryotic homologous proteins,[10,19−21] yet an understanding of how these domains are arranged in the functional NO sensor remains unknown.

Small molecule stimulators of sGC have been discovered, opening new doors for drug discovery in the treatment of cardiovascular diseases.[22] The first of these is compound YC-1, a benzylindazole derivative that inhibits platelet activation through stimulating sGC.[23] YC-1 stimulates sGC 2−4-fold in the absence of NO but acts synergistically with CO or NO to achieve several hundred-fold activation.[24,25] Binding of YC-1 can also overcome the inhibitory phosphorylation of sGC.[26] Compound BAY 63-2521 (riociguat), a YC-1 derivative, has just completed phase III clinical trials[27−30] and has been approved by the Food and Drug Administration for treatment of pulmonary hypertension (as Adempas). These compounds stimulate sGC activity in an NO-independent and heme-dependent manner, but how they bind to sGC and how they stimulate catalytic activity are unknown. Studies aimed at determining the binding site for YC-1 family compounds have suggested the pseudosymmetric site in the cyclase domain,[31,32] the α_1 H-NOX domain,[33,34] and the β_1 H-NOX domain.[35−38] A second class of compounds that function through replacing the sGC heme, which can be lost upon oxidation, have also been developed.[22] Prominent among these are compounds BAY 58-2667 (cinaciguat)[39] and HMR1766 (ataciguat).[40]

We developed sGC from the tobacco hornworm/hawkmoth (*Manduca sexta*) for biophysical and biochemical characterization and to help with uncovering the mechanism underlying YC-1 stimulation.[33,41−43] *M. sexta* sGC (*Ms* sGC) is highly homologous to its mammalian counterparts and responds well to YC-1 family compounds. Expression of N-terminal heterodimeric constructs lacking the α_1/β_1 cyclase domains (*Ms* sGC-NT constructs) leads to proteins that preserve YC-1 binding. Binding of YC-1 to *Ms* sGC leads to enhanced CO and NO binding[33] and to the trapping of CO in the heme pocket after laser photolysis, leading to rebinding with heme before escape from the protein (geminate recombination).[41] *Ms* sGC-NT is an elongated molecule with a central parallel coiled-coil domain, based on chemical cross-linking, mass spectrometry, and small-angle X-ray scattering (SAXS) studies.[43] In this model, the coiled-coil domain acts as an organizing center for the PAS, H-NOX, and, presumably, cyclase domains. Here, we demonstrate that the α subunit serves to keep the β subunit heme domain in a conformation with reduced affinity for CO and that YC-1 binds directly to the β subunit, inducing a high-affinity heme domain conformation.

EXPERIMENTAL PROCEDURES

Materials. All chemicals were obtained from Sigma-Aldrich, restriction enzymes from Fermentas, and purification columns from GE Healthcare unless otherwise indicated. Pfizer compound 25 targeted to sGC (PF-25) was kindly provided by L. Roberts of Pfizer Inc.[44] DEA/NO was kindly provided by K. Miranda (The University of Arizona).

sGC Protein Expression Vectors. Construct *Ms* sGC CT1 (α_1 residues 272−699 and β_1 residues 199−600) was obtained by polymerase chain reaction (PCR) amplification from a full-length *Ms* sGC pETDuet1 construct.[33] Forward primer 5′-ggatccgaccaaagtgacagattt-3′ and reverse primer 5′-gcggccgcctaagttggttcttct-3′ were used for the α_1 subunit, and the PCR product was cloned into the pETDuet1 vector using the BamHI and NotI restriction sites. Similarly, the *Ms* sGC CT1 β_1 fragment was obtained by PCR amplification from the *Ms* sGC full-length pETDuet1 construct using primers 5′-catatgacgttgtctcttgaacca-3′ and 5′-gatatcttaatggatcttcctggt-3′, and the PCR product was cloned into the same pETDuet1 vector using the NdeI and EcoRV restriction sites. The final construct had a His_6 purification tag fused to the N-terminus of the α_1 subunit. Stop codons were inserted at α_1 Asn 451 and β_1 Thr 381 using the QuikChange lightning site-directed mutagenesis kit (Stratagene, La Jolla, CA), leading to constructs containing just the PAS and coiled-coil domains (α_1 residues 272−450 and β_1 residues 199−380).

Possible boundaries for stable PAS domain expression were surveyed using the *Ms* sGC α_1 PAS-CC-cyclase (residues 272−699) and β_1 PAS-CC-cyclase (residues 199−600) cloned into a single plasmid (pETDuet-1, Novagen) or cloned individually into the pETDuet-1 (α_1) or pET28a+ (β_1) plasmid. Domain boundaries were examined through introduction of stop codons, using the QuikChange mutagenesis kit. The *Ms* sGC β_1 PAS construct (residues 199−319) in pET28a+ was obtained by inserting a stop codon at position 320. The *Ms* sGC α_1 PAS domain, spanning residues 279−425, was cloned into the pETHSUL vector, kindly provided by the Loll laboratory.[45] A ligation-independent cloning (LIC) approach was undertaken as described previously,[45] using forward primer 5′-agattggtggcatcggcgtggctagcttctgc-3′ and reverse primer 5′-gaggagagtttagacttaaccatcctgagccctagcc-3′ (LIC overhang residues are underlined). The vector was made ready for ligation using the direct digestion method with BseRI (New England Biolabs). A stop codon was introduced at position 405 to yield wild-type construct *Ms* sGC-P25α, spanning residues 279−404. A triple cysteine-to-alanine mutant (C285A/C352A/C374A, *Ms* sGC-P35α) was produced to assist in crystallization.[17] All mutations were introduced using the QuikChange lightning site-directed mutagenesis kit. Vector pSUPER, containing a dual-tagged catalytic domain of SUMO hydrolase (dtUD1) fused to the N-terminus of SUMO, was also kindly provided by the Loll laboratory.[45] *Ms* sGC β_1(1−380), containing the H-NOX and PAS domains and most of the CC domain, was amplified by PCR and subcloned into the pGEM-T vector. The fragment was then cut with the restriction enzymes NcoI and NotI and inserted into the pET28c vector, yielding a C-terminal His_6 tag.

A single-step insertion methodology[46] was used for insertion of the BirA recognition sequence (Avi-tag, GLNDIFEAQKIEWHE) at the C-terminus of the *Ms* sGC-NT21 β_1 subunit (residue 380, ref 43) and *Ms* sGC β_1(1−380) using forward primers 5′-ggaattggaaaaacagaagggtggcggtctgaacgacatcttcgaggctcaaaaaatagagtggcacgagtaggacaggcttctttactcagtg-3′ and 5′-ggaattggaaaaacagaagggtggcggtctgaacgacatcttcgaggctcaaaaaatagagtggcacgaggcggccgcactcgagcaccaccac-3′ and common reverse primer 5′-cttctgtttttccaattccagctctcggaatgtttgttgaag-3′. The Avi tags with two N-terminal glycine linker residues are underlined. Similarly, a C-terminal Avi tag was added to α_1 PAS domain construct *Ms* sGC-P25α using forward primer 5′-gactcttcatatccgatataggtggcggtctgaacgacatcttcgaggctcaaaaaatagagtggcacgagtgacttcatgatgcgacgagag-3′ and reverse primer 5′-tatatcggatatgaagagtccccttccagtcagaccttcgag-3′. *Escherichia coli* biotin protein ligase BirA in vector pGEX-4T-1, with an N-terminal GST tag linked to a thrombin cleavage site and a C-terminal His_6 tag,

was kindly provided by M. Kuhns (The University of Arizona). The thrombin cleavage site was changed to a TEV cleavage site using forward primer 5′-ccatcctccaaaatcgggcgaaaacttgtatttccaggatccaaggataacaccg-3′ and reverse primer 5′-cggtgttatccttggatccctggaaatacaagttttcgcccgattttggaggatgg-3′ (TEV cleavage site underlined). Additionally, a stop codon was inserted in front of the His_6 tag.

Expression and Purification of *Ms* sGC PAS Domains. *Ms* sGC α_1 PAS with an N-terminal His-tagged SUMO fusion was expressed in *E. coli* strain BL21(DE3) pLysS. Cells were grown at 37 °C to an OD_{600} of 0.6 before being induced with 0.5 mM isopropyl 1-thio-β-D-thiogalactopyranoside (IPTG) and then grown at 20 °C; cells were harvested after 16 h. Purification steps were performed at 4 °C. Cell pellets were resuspended in lysis buffer [50 mM sodium phosphate (pH 7.4), 300 mM NaCl, 20 mM imidazole, 0.1 mg/mL DNase I, 2 mM $MgCl_2$, 1 mM phenylmethanesulfonyl fluoride (PMSF), 1 mM benzamidine, and 1 μg/mL aprotinin, leupeptin, and pepstatin], disrupted using a French press cell (1000 psi), clarified by ultracentrifugation (45Ti rotor, 40000 rpm for 30 min), supplemented with 10% glycerol (w/v) and 5 mM β-mercaptoethanol, and loaded onto a 5 mL Ni-NTA column previously equilibrated with binding buffer [50 mM sodium phosphate (pH 7.4), 300 mM NaCl, 20 mM imidazole, and 5 mM β-mercaptoethanol]. The column was washed with binding buffer until the baseline was reached, and bound protein was eluted using an imidazole gradient ranging from 20 to 300 mM over 100 mL (20 bed volumes) by mixing binding buffer and elution buffer (binding buffer supplemented with 500 mM imidazole). Cleavage of the N-terminal His-tagged SUMO domain was achieved by adding 1 mg of purified SUMO hydrolase (dtUD1) to the pooled PAS-containing fractions followed by overnight dialysis at 4 °C against two changes of dialysis buffer [50 mM sodium phosphate (pH 7.4), 300 mM NaCl, 5% glycerol (w/v), and 10 mM β-mercaptoethanol]. The dialyzed product was again loaded onto the Ni-NTA column to remove the His-tagged SUMO and SUMO hydrolase proteins, followed by concentration to ∼3 mL and further purification over an S-200 size exclusion column previously equilibrated with equilibration buffer [50 mM Tris-HCl (pH 7.4), 200 mM NaCl, 5% glycerol (w/v), and 5 mM dithiothreitol]. The final material was concentrated to 10−15 mg/mL using a Vivaspin concentrator (Sartorius Stedim Biotech) and stored at −80 °C. A final yield of 2−3 mg of highly pure protein was obtained per liter of cell culture.

Ms sGC β_1 PAS was expressed in *E. coli* strain Rosetta pLysS. Cells were grown at 37 °C to an OD_{600} of 1.0 and induced with 0.2 mM IPTG, after which they were grown while being slowly shaken (90 rpm) at 18 °C for 18 h before being harvested. The cell lysate was obtained as described for the α_1 PAS domain, and the protein was purified using Ni-NTA followed by S-200 size exclusion chromatography. A yield of 30−40 mg was obtained per liter of cell culture.

SUMO hydrolase (dtUD1) was expressed in strain BL21-(DE3) pLysS. Cells were grown at 37 °C until the OD_{600} reached 0.6, induced with 0.5 mM IPTG, and grown at 30 °C for 6 h before being harvested. Purification was performed using Ni-NTA column chromatography as described previously.[45]

BirA was expressed in strain BL21(DE3) pLysS. Cells were grown at 37 °C to an OD_{600} of 1.0, and expression was induced with 0.5 mM IPTG, followed by growth at 16 °C for 20 h before being harvested. Cells were lysed by sonication at 4 °C in lysis buffer and clarified by ultracentrifugation, and the supernatant was loaded onto a GSTrap FF column previously equilibrated with 50 mM sodium phosphate buffer (pH 7.4) containing 300 mM NaCl. Bound GST-tagged BirA was eluted with the buffer described above supplemented with 20 mM glutathione. Fractions were incubated for 24 h with 5 μM His_6-tagged TEV protease, and the mixture was loaded onto a GSTrap FF column in tandem with a Ni-NTA column. The flow through was collected and the protein concentrated and stored at −80 °C.

TEV protease with N-terminal polyhistidine, C-terminal polyarginine, and mutation S219V was prepared from a previously described pRK793 vector.[47] TEV protease was expressed in *E. coli* strain BL21(DE3) pLysS. Cells were grown to an OD_{600} of 0.6 at 37 °C, induced with 1 mM IPTG, and grown at 30 °C for 6 h before being harvested. Cell pellets were resuspended in binding buffer [50 mM sodium phosphate (pH 7.4), 300 mM NaCl, and 20 mM imidazole], disrupted using a French press cell (1000 psi), and clarified by ultracentrifugation (45Ti rotor, 40000 rpm for 30 min). The supernatant was supplemented with 10% glycerol (w/v) and 5 mM β-mercaptoethanol before being loaded onto a 5 mL Ni-NTA column previously equilibrated with binding buffer [50 mM sodium phosphate (pH 7.4), 300 mM NaCl, 20 mM imidazole, and 5 mM β-mercaptoethanol]. The column was washed with binding buffer until the baseline was reached, and bound protein was eluted using an imidazole gradient ranging from 20 to 300 mM over 100 mL (20 bed volumes) by mixing binding buffer and elution buffer (binding buffer supplemented with 500 mM imidazole). Fractions containing TEV protease were pooled, buffer exchanged with final storage buffer [50 mM sodium phosphate (pH 7.4), 300 mM NaCl, 25% glycerol, 1 mM EDTA, and 1 mM DTT], concentrated to a final concentration of ∼4 mg/mL, and frozen at −80 °C.

Expression and Purification of Heme-Containing *Manduca* and Bovine sGC Proteins. *Ms* sGC-NT13, *Ms* sGC-NT19, and *Ms* sGC-NT21 were expressed in *E. coli* and purified using Ni-NTA, StrepTactin (*Ms* sGC-NT19), and size exclusion chromatography, as previously described.[33,43] *Ms* sGC β_1(1−380) was expressed in *E. coli* strain Rosetta pLysS. Cells were grown at 37 °C to an OD_{600} of 1.0 and cooled on ice before being induced. The culture was induced with 0.5 mM IPTG, supplemented with 25 μM δ-aminolevulinic acid, and grown at 30 °C for 6 h before being harvested. Cell pellets were resuspended in lysis buffer B [50 mM Tris-HCl (pH 8.5), 10 mM NaCl, 0.1 mg/mL DNase I, 2 mM $MgCl_2$, 1 mM PMSF, 1 mM benzamidine, 1 μg/mL aprotinin, 1 μg/mL leupeptin, 1 μg/mL pepstatin, and 1 mM dithionite], disrupted with a French pressure cell, and clarified by ultracentrifugation. The supernatant was supplemented with 10% (w/v) glycerol, 5 mM β-mercaptoethanol, and an ∼100-fold excess of dithionite (∼1 mM, assuming 2 mg of protein/L of cell culture). The sample was loaded onto a DEAE anion exchange column or Q-FF Sepharose column previously equilibrated with buffer A [20 mM Tris-HCl (pH 8.5), 1 mM EDTA, and 5 mM β-mercaptoethanol], the column washed with buffer A, and protein eluted with a 0 to 300 mM NaCl elution gradient (200 mL) using buffer A (0 mM NaCl) and buffer B (buffer A with 500 mM NaCl). Colored fractions were pooled and loaded onto the Ni-NTA column and eluted with 30 mM EDTA in a single-step elution. Fractions were supplemented with fresh dithionite and tris(2-carboxyethyl)phosphine (TCEP), concentrated, and further purified by being run through a size

dx.doi.org/10.1021/bi4015133 | *Biochemistry* 2014, 53, 101−114

exclusion S200 column previously equilibrated with gel filtration buffer [50 mM potassium phosphate buffer (pH 7.4), 100 mM KCl, 2 mM EDTA, 5% glycerol, and 1 mM TCEP], where it ran as a monomer. The purified protein was supplemented with dithionite, concentrated to 5−10 mg/mL, and stored at −80 °C.

For the bovine sGC β_1 H-NOX and β_1 H-NOX-PAS, we used a systematic site-directed mutagenesis approach to determine the appropriate C-terminal ends for optimal expression and solubility of the proteins (J. Hines, L. Rassouli-Taylor, J. Burstyn, and E. Garcin, Raman studies of bovine soluble guanylate cyclase, manuscript in preparation). We used the untagged β_1(1−385) (residues 1−385) construct cloned into the pET30b plasmid (kind gift of J. Burstyn) and introduced stop codons at various positions using the QuikChange mutagenesis kit. *Bt* sGC β_1 H-NOX (residues 1−197) and sGC β_1 H-NOX-PAS (residues 1−359) in pET30b were obtained by inserting a stop codon at positions 198 and 360, respectively. These constructs displayed the highest levels of expression and solubility in *E. coli* cells. Purification of both constructs was performed as follows. Each construct was expressed in *E. coli* strain BL21(DE3) pRIPL. Cells were grown at 37 °C to an OD_{600} of 1.0 and cooled on ice before being induced. The culture was induced with 0.4 mM IPTG, supplemented with 450 μM δ-aminolevulinic acid and ferric citrate, and grown at 20 °C for 24 h before being harvested. Cell pellets were resuspended in lysis buffer [20 mM Tris-HCl (pH 7.5), 50 mM NaCl, DTT, 0.5 mg/mL lysozyme, 300 units of benzonase (SIGMA), and one tablet of EDTA-free protease inhibitor cocktail tablet/50 mL (Roche)], disrupted by sonication, and clarified by ultracentrifugation. We used 10 mM DTT to keep the β_1 H-NOX protein reduced and 1 mM DTT for the β_1 H-NOX-PAS construct. The clarified lysate was loaded onto a Q-FF Sepharose column previously equilibrated with buffer A [20 mM Tris-HCl (pH 7.5), 50 mM NaCl, and DTT], and the protein was eluted with a 0.05 to 1 M NaCl elution gradient (buffer B being buffer A with 1 M NaCl). Colored fractions were pooled, dialyzed into buffer A, and loaded onto an S75 size exclusion column equilibrated in buffer A. Colored fractions were pooled and loaded onto a second QFF column pre-equilibrated in buffer C [20 mM Tris-HCl (pH 8.5), 50 mM NaCl, and TCEP]. The protein was eluted with a 0.05 to 1 M NaCl gradient (buffer D being buffer C with 1 M NaCl). The colored fractions were pooled and dialyzed into buffer C (10 and 1 mM TCEP for β_1 H-NOX and β_1 H-NOX-PAS, respectively). The purified protein was concentrated to ∼10 mg/mL and stored at −80 °C.

Determination of Dissociation Constants for CO. CO dissociation constants were measured by titrating CO from a saturated solution into sGC protein and monitoring the appearance of the CO-bound Soret absorption band, as described previously.[33,43] The *Ms* sGC β_1(1−380) and *Bt* sGC β_1(1−197) samples were prepared in Ar-purged buffer supplemented with excess dithionite. CO binding experiments were performed in a 10 cm path length cuvette for *Ms* sGC-β_1(1−380) and *Ms* sGC-NT21 using a Cary 50 spectrophotometer (Varian) with a modified sample holder. Binding data in the presence and absence of 50 μM YC-1 were plotted using a single-site saturation ligand binding model in SigmaPlot (SPSS, Inc., Chicago, IL).

To extract linked equilibrium binding behavior, CO binding assays were performed for *Ms* sGC-NT21 (10 cm cuvette) and *Ms* sGC-NT13 (1 cm cuvette) at various YC-1 concentrations. The stimulation of CO binding in the presence of YC-1 was described with a cooperative two-site model with four states: free protein, protein bound to CO only, protein bound to YC-1 only, and protein bound to both CO and YC-1. Independent binding of CO and independent binding of YC-1 are described with association constants K_a^{CO} and $K_a^{YC\text{-}1}$, respectively, with an assumed cooperativity constant K_{int} representing coupling between the two binding processes. This model is described with a binding polynomial of the form

$$Z = 1 + K_a^{CO}[CO] + K_a^{YC\text{-}1}[YC\text{-}1] + (K_a^{CO}[CO])(K_a^{YC\text{-}1}[YC\text{-}1])K_{int} \quad (1)$$

in which each term represents the statistical weight for one of the four states. The fraction of CO sites occupied is given by the ratio of the weights for states with CO bound to all four states:

$$\theta = [K_a^{CO}[CO] + (K_a^{CO}[CO])(K_a^{YC\text{-}1}[YC\text{-}1])K_{int}]/Z \quad (2)$$

Estimates for the model parameters K_a^{CO}, $K_a^{YC\text{-}1}$, and K_{int} were obtained from a global fit of θ to the normalized absorbance changes at wavelengths of 423 and 433 nm, using MATLAB (The MathWorks, Inc., Natick, MA). The product $K_a^{YC\text{-}1}K_{int}$ indicates the association constant for binding of YC-1 to the CO-bound complex, so its inverse represents the dissociation constant $K_d^{YC\text{-}1'}$. Similarly, $K_d^{CO'}$ may be estimated from the inverse of the product $K_a^{CO}K_{int}$.

To directly measure the binding of YC-1 family compounds to *Ms* sGC-NT-CO, an ∼2 nm shift in the Soret band maxima was monitored as a function of compound concentration. The compound was titrated into a 1 or 10 cm cuvette containing a CO-saturated protein solution. The K_d for ligand binding in the presence of CO was calculated by plotting the Soret shift difference with respect to the increasing concentrations of the ligand and fitting to a single-site saturation ligand binding model in SigmaPlot.

Fluorescence Anisotropy. Fluorescence anisotropy was measured using a JASCO J-815 CD fluorescence spectrometer equipped with an anisotropy attachment (JASCO). Average anisotropy was measured at 20 °C for 60 s using an excitation wavelength of 325 nm. Anisotropy was calculated using total fluorescence above 380 nm, which was measured 90° incident to the excitation beam. Initial anisotropy was measured for a 2 μM YC-1 solution in 10 mM Tris-HCl (pH 7.5) by titrating *Ms* sGC α_1 P25α or β_1 PAS or lysozyme, and the sample was mixed thoroughly for 30 s before anisotropy measurements were taken. Data were fit using a one-site total binding model implemented in GraphPad (GraphPad Software, Inc.).

Surface Plasmon Resonance Binding Experiments. *In vitro* biotinylation of Avi-tagged *Ms* sGC-NT21, *Ms* sGC α_1 PAS, and *Ms* sGC β_1(1−380) was performed using *E. coli* BirA biotin ligase. A reaction mixture containing 30−40 μM Avi-tagged protein, 1−2 μM purified BirA, 0.5 mM biotin, 10 mM magnesium acetate, and 10 mM ATP was incubated at 4 °C for 6 h and loaded onto a Ni-NTA column (*Ms* sGC-NT21) or Superdex-75 analytical gel filtration column [*Ms* sGC α_1 PAS and *Ms* sGC β_1(1−380)] to remove excess reaction components. Biotinylation was confirmed by a monoclonal anti-biotin antibody (Sigma-Aldrich) Western blot. All SPR studies were performed on a Biacore T100 instrument at 20 °C. Both reference and sample CM5 sensor chip surfaces (GE Healthcare) were prepared by an amine coupling methodology

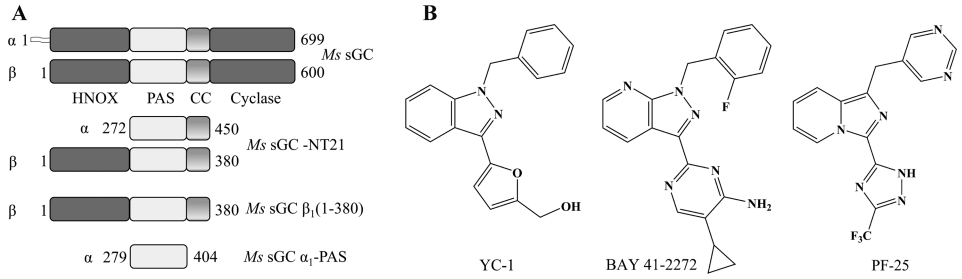

Figure 1. sGC constructs and ligand structures. (A) Schematic representation of the heterodimeric *Ms* sGC domains, expression constructs, and their boundaries. Constructs used in this study but not shown in the diagram are *Ms* sGC-NT13 (α_1 residues 49−450 and β_1 residues 1−380), *Bt* sGC β_1(1−197), and *Bt* sGC β_1(1−359). (B) Structures of YC-1, BAY 41-2272, and PF-25.

following the procedures in the Biacore T100 instrument manual. The chip surfaces were first activated by using a mixture of *N*-hydroxysuccinimide (NHS) and 1-ethyl-3-[3-(dimethylamino)propyl]carbodiimide (EDC). NeutrAvidin (Pierce), 100 μg/mL in 10 mM NaOAc (pH 4.5), was then immobilized to 10000 response units by passing it over the activated surfaces. Running buffer consisted of 10 mM HEPES (pH 7.4), 150 mM NaCl, 1 mM EDTA, and 0.05% Tween 20. Any remaining active esters were blocked with ethanolamine, and the immobilized NeutrAvidin chip surface was washed three times with a 30 s pulse of 10 mM HCl. Biotinylated *Ms* sGC proteins were captured onto the NeutrAvidin-coated chip surfaces by injecting 25 μM protein at a flow rate of 10 μL/min until ∼10000 response units had been achieved. Running buffer consisted of 50 mM potassium phosphate buffer (pH 7.4), 100 mM KCl, 2 mM EDTA, and 1 mM TCEP. The surfaces were washed with running buffer for 2 h at a flow rate of 100 μL/min until a stable response was obtained, indicating no further dissociation of the biotinylated proteins. Each chip has four flow cells allowing simultaneous measurements on one reference and three active surfaces. The Biacore T100 MIX function was used to mix DEA/NO or NaOH alone (0.5 mM DEA/NO stock in 10 mM NaOH and 1% DMSO, contained in an Ar-purged sealed Biacore vial) with varied concentrations of PF-25 in 50 mM potassium phosphate buffer (pH 7.4), 100 mM KCl, 2 mM EDTA, and 1 mM TCEP containing 1% DMSO to achieve a final DEA/NO concentration of 25 μM. Various concentrations of PF-25 containing DEA/NO or NaOH were injected over the surface at a rate of 25 μL/min with 115 s association and 240 s dissociation times. Running buffer consisted of 50 mM potassium phosphate buffer (pH 7.4), 100 mM KCl, 2 mM EDTA, 1 mM TCEP, and 1% DMSO. Solvent correction curves were used to compensate for any mismatch between the sample buffer and the running buffer. Data were analyzed with Biacore T100 evaluation software to obtain the offset corrected response [*R*, measured in response units (RU)] and the expected maximal response (R_{max}) based on the response from the immobilized protein (R_{immob}) and the relative molecular weights of ligand and analyte:

$$R_{max} = (\text{MW PF-25}/\text{MW protein})\, R_{immob}(\text{stoichiometric ratio}) \quad (3)$$

For measurements in cases in which binding was very weak (−NO), the dissociation constant was obtained from a single-site saturation ligand binding model with R_{max} constrained, while for tighter binding (+NO), R_{max} was allowed to be fit. Fitting was conducted with SigmaPlot:

$$R = (R_{max}[\text{PF-25}])/(K_d + [\text{PF-25}]) + \text{offset} \quad (4)$$

RESULTS

The sGC α Chain Inhibits CO Capture by Heme in the β Chain. To begin to understand how the affinity of NO and CO for sGC heme is modulated, we examined binding of CO to a variety of sGC proteins lacking specific domains but retaining heme. Measurements were taken in the presence or absence of YC-1 or related compounds. We focused on CO binding because its affinity for ferrous heme was lower than that of NO, allowing for the measurement of equilibrium dissociation constants, and because of its clear response to YC-1 binding. Measurements were taken with *Ms* sGC-NT constructs (Figure 1), taking advantage of their high stability and high yields from bacterial expression.[33,41−43] *Ms* sGC-NT constructs are heterodimeric proteins lacking the C-terminal cyclase domains while retaining YC-1 binding. We previously demonstrated that YC-1 binding leads to tighter CO and NO binding and to a geminate recombination phase upon CO photolysis.[33,41] Here, we extend these studies to include proteins completely lacking the α_1 chain and, where needed, using a cuvette with a path length of 10 cm, allowing for more precise measurement of the tighter binding constants that occur in the presence of YC-1 (Figure 2 and Table 1).

The *Ms* sGC coiled-coil domain likely ends at α_1 Pro 460 and β_1 Pro 390.[16,42,43] We trimmed the C-terminal end of *Ms* sGC-NT2 by 21 residues to remove a portion of the linker between the coiled-coil and cyclase domains, as well as a small portion of the coiled-coil domain, yielding *Ms* sGC-NT13 and *Ms* sGC-NT19, which are identical except for addition of a *Strep* purification tag to *Ms* sGC-NT19. Both proteins display a small increase in CO binding affinity in the absence of YC-1, but no significant change in CO affinity in the presence of YC-1 (Table 1). Values for K_d^{CO} obtained with these proteins varied from 50−90 μM in the absence of YC-1 to 0.8−2.8 μM in the presence of YC-1 (termed $K_d^{CO\prime}$). Removal of the α_1 H-NOX domain (*Ms* sGC-NT21) led to considerable tightening of CO binding [K_d^{CO} = 2.2 μM, and $K_d^{CO\prime}$ = 0.2 μM (Table 1)]. These measurements were taken in a 10 cm cuvette, allowing protein concentrations as low as 50 nM to be used and minimizing the depletion of free CO through heme binding. Thus, *Ms* sGC-NT21 binds CO 20−40-fold tighter than *Ms* sGC proteins containing the α_1 H-NOX domain and still responds to YC-1, displaying a 10-fold increase in CO binding affinity when YC-1 is present. These data are consistent with previous studies indicating YC-1 family compounds stimulate NO-dependent catalysis in sGC proteins lacking the first 259 residues of α_1.[48−50]

dx.doi.org/10.1021/bi4015133 | *Biochemistry* 2014, 53, 101−114

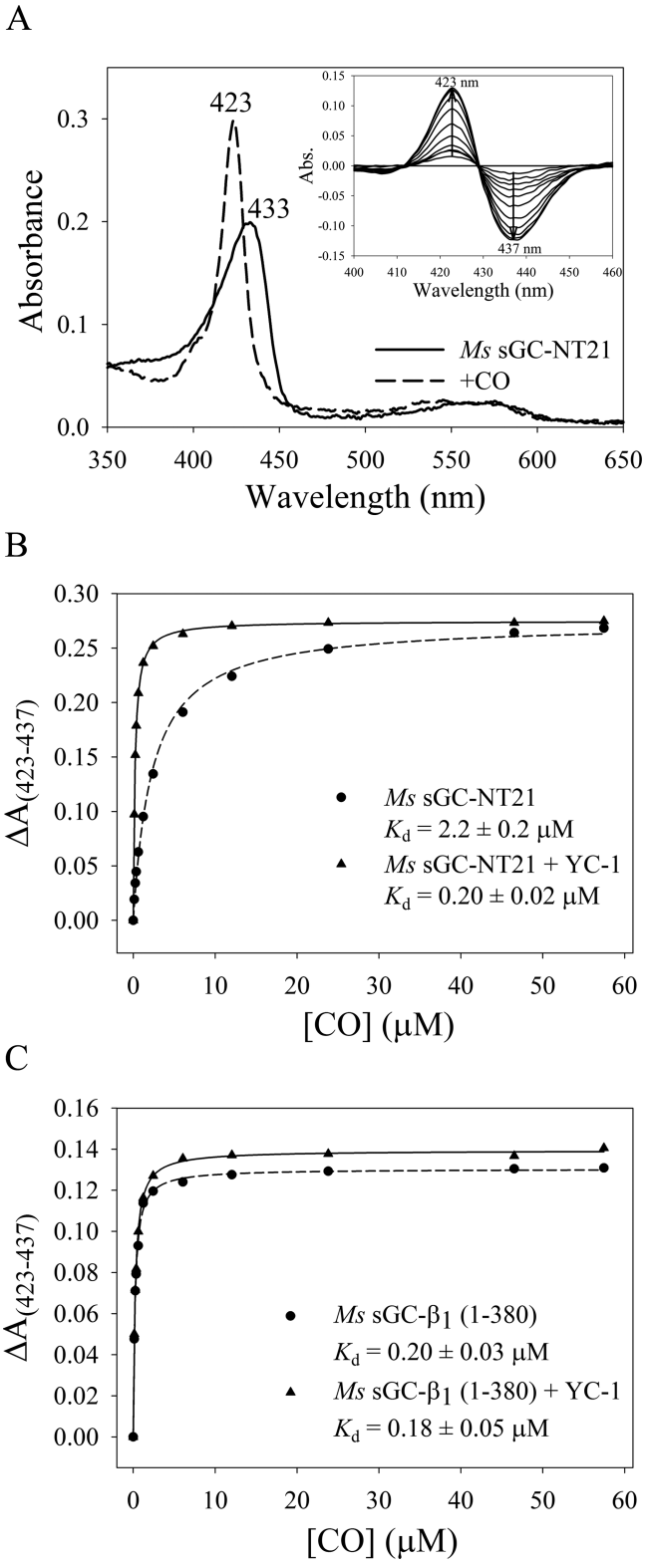

Figure 2. CO saturation binding analysis. (A) Absorption spectra of purified *Ms* sGC-NT21 before and after CO saturation. The A_{433}/A_{280} ratio for the unliganded protein is ~1.8, consistent with high purity and full heme incorporation. The inset shows difference spectra for *Ms* sGC-NT21 upon CO titration. (B) CO saturation binding curve for *Ms* sGC-NT21 with or without YC-1, which displays a 10-fold tightening of the CO dissociation constant upon YC-1 binding. (C) CO saturation binding curve for *Ms* sGC-β_1(1−380) with or without YC-1, which displays little change in CO binding affinity upon YC-1 binding. Titrations were performed in a 10 cm cuvette at room temperature with 0.1 μM protein in buffer containing 50 mM potassium phosphate (pH 7.4), 100 mM KCl, 5% glycerol, and 50 μM YC-1. The data were corrected for dilution upon addition of CO-saturated buffer and were fit to a single-site saturation model to obtain the CO dissociation constants.

To further narrow the YC-1 binding location, we examined an *Ms* sGC protein lacking the entire α_1 chain. This protein binds CO with high affinity (~0.2 μM) in the presence or absence of YC-1 (Figure 2 and Table 1). Thus, YC-1 appears to have no effect on CO binding affinity in the absence of the α chain, and importantly, CO binding is as tight in the absence of the α chain as it is in the presence of YC-1 for any of the heterodimeric *Ms* sGC proteins, displaying a K_d^{CO} value of ~200 nM. We conclude that both the α_1 PAS and H-NOX domains lower the CO affinity for the sGC heme. Binding of YC-1 appears to relieve this restraint.

We examined the bovine β_1 subunit to extend our results to a mammalian sGC. The bovine protein displays the same overall domain structure as *Ms* sGC and has an overall level of sequence identity of 60% with the β_1 subunit and 39% with the α_1 subunit. We produced two *Bt* sGC forms, one containing just the H-NOX domain and one containing the H-NOX and PAS domain. As with *Ms* sGC β_1, neither *Bt* sGC β_1 construct displayed YC-1 sensitivity (Table 1). Binding of CO to the bovine protein was less tight, however, and differed between the H-NOX domain- and H-NOX-PAS domain-containing proteins, with the shorter construct having the greatest affinity (~1 μM) and the longer construct binding with ~10-fold less affinity. Homodimer formation in *Bt* sGC β_1(1−359) may contribute to the lower CO affinity [*Ms* sGC β_1(1−380) behaves as a monomer].

Binding Affinity of YC-1 for *Ms* sGC. The data in Table 1 indicate the YC-1 binding site is within the *Ms* sGC-NT21 construct and, furthermore, that YC-1 enhancement of CO binding requires an intact α_1 PAS domain. Measurement of the binding affinity of YC-1 for sGC, which is needed to clarify where on the protein binding takes place, is frustrated by the poor solubility of YC-1 in aqueous solutions and by the tendency for YC-1 to bind nonspecifically to proteins. We therefore employed a multidimensional binding assay to extract the YC-1 dissociation constant through analysis of the linked equilibria between CO binding and YC-1 binding (Figure 3 and Table 2). For a system displaying linked equilibria, binding of either ligand, in this case CO or YC-1, will affect the binding of the other. We therefore measured CO binding affinity as a function of YC-1 concentration for *Ms* sGC-NT21 (10 cm cuvette) and *Ms* sGC-NT13 (1 cm cuvette). Linked equilibrium analyses yielded $K_d^{YC\text{-}1}$ values of 9.3 and 21 μM, respectively, for the two proteins in the absence of NO and CO (Table 2). Cooperativity factors of 14 and 19 (Table 3), reflecting the influence of one ligand on binding of the other, were also derived from these data, from which the dissociation constant for the binding of YC-1 to the CO-saturated protein ($K_d^{YC\text{-}1\prime}$) can be derived. These values were 0.7 and 1.1 μM for *Ms* sGC-NT21 and *Ms* sGC-NT13, respectively (Table 2).

We also directly measured binding of YC-1 to CO-saturated heterodimeric *Ms* sGC proteins by monitoring the ~2 nm blue shift in the Soret absorption band that occurs upon YC-1 binding.[41,51] Monitoring of this shift while titrating in YC-1 allowed the estimation of compound affinity (Figure 4, Table

dx.doi.org/10.1021/bi4015133 | *Biochemistry* 2014, 53, 101−114

Table 1. CO Dissociation Constants for sGC Proteins[a]

protein	α_1 residues	β_1 residues	K_d^{CO} (μM)	$K_d^{CO\prime}$ (μM) (ligand)	ref
Bt sGC (full length)	1–691	1–619	127	~26 (YC-1)	51
			97		76
Hs sGC (full length)	1–690	1–619	260		77
Ms sGC-NT2	49–471	1–401	77 ± 7	1.7 ± 0.1 (YC-1)	33
			90 ± 9	1.0 ± 0.1 (YC-1)	43
Ms sGC-NT13	49–450	1–380	53 ± 4	2.8 ± 0.4 (YC-1)	this work
				2.9 ± 0.2 (PF-25)	this work
				0.25 ± 0.02[b] (BAY)	this work
Ms sGC-NT19	49–450	1–380	50 ± 3	0.8 ± 0.1 (YC-1)	43
Ms sGC-NT21	272–450	1–380	2.2 ± 0.2[b]	0.20 ± 0.02[b] (YC-1)	this work
				0.24 ± 0.01[b] (PF-25)	this work
				0.07 ± 0.01[b] (BAY)	this work
Ms sGC β_1(1–380)	absent	1–380	0.20 ± 0.03[b]	0.18 ± 0.05[b] (YC-1)	this work
Bt sGC β_1(1–197)	absent	1–197	1.6 ± 0.2[c]	1.2 ± 0.2[c] (YC-1)	this work
Bt sGC β_1(1–359)	absent	1–359	15 ± 4	10 ± 3 (YC-1)	this work

[a]Titration binding data were measured using gastight syringes and 1 or 10 cm cuvettes fitted with rubber septa. The protein concentration was 1 μM unless otherwise indicated. Where included for measuring $K_d^{CO\prime}$, the YC-1 and PF-25 concentrations were 50 μM and the BAY 41-2272 concentration was 2.5 μM (*Ms* sGC-NT21) or 10 μM (*Ms* sGC-NT13). Values are means and the standard deviation of at least three independent measurements. [b]Measured in a 10 cm cuvette, using 0.1 μM protein. [c]Measured in a 1 cm cuvette, using 0.5 μM protein.

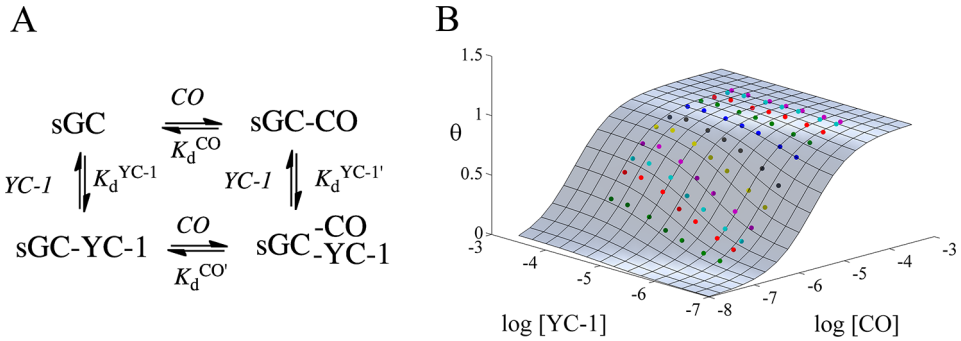

Figure 3. Ligand binding and linked equilibria in sGC. (A) Linked equilibrium diagram showing four different states for binding of CO and YC-1 to sGC. (B) Global fitting of the fraction of CO sites occupied (θ) to the normalized $\Delta A_{(423-437)}$ for *Ms* sGC-NT21 (10 cm cuvette) using MATLAB. The surface represents the extent of CO binding as a function of CO and YC-1 concentration. Colored points indicate the measured $\Delta A_{(423-437)}$. Titrations were performed in a 10 cm cuvette at room temperature with 0.1 μM protein in buffer containing 50 mM potassium phosphate (pH 7.4), 100 mM KCl, 5% glycerol, and YC-1 concentrations ranging from 0 to 50 μM.

Table 2. YC-1, PF-25, and BAY 41-2272 Dissociation Constants for sGC Proteins (micromolar)

	without NO or CO			with CO			with NO
protein	K_d^{YC-1}	K_d^{PF-25}	K_d^{BAY}	$K_d^{YC-1\prime}$	$K_d^{PF-25\prime}$	$K_d^{BAY\prime}$	$K_d^{PF-25\prime}$
Ms sGC-NT13	21 ± 5[a]	155 ± 11[a]	17 ± 3[b]	1.1 ± 0.3[a]	3.0 ± 0.3[a]	0.08 ± 0.01[e]	
				0.8 ± 0.1[d]	2.8 ± 0.2[d]		
Ms sGC-NT21	9.3 ± 0.8[a]	73 ± 21[a]	2.0 ± 0.5[a]	0.67 ± 0.06[a]	3.8 ± 1.4[a]	0.03 ± 0.01[a]	11 ± 2[c]
		153 ± 5[c]		0.6 ± 0.1[e]	0.9 ± 0.3[d]	0.09 ± 0.02[e]	
Ms sGC β_1(1–380)		92 ± 5[c]					7 ± 1[c]
Ms sGC α_1 PAS		NB[c]					NB[c]
Bt sGC (full length)	52[f]			~8[h]			
	~20[g]						

[a]From global fitting of multidimensional titration data (see the text). For *Ms* sGC-NT13, titration occurred in a 1 cm cuvette with 1 μM protein. For *Ms* sGC-NT21, titration occurred in a 10 cm cuvette with 0.1 μM protein. Values are means and the standard deviation of three independent measurements. Values for $K_d^{YC-1\prime}$ were obtained using the cooperativity factors listed in Table 3. [b]Estimated assuming linked equilibria: $(K_d^{CO}/K_d^{CO\prime})K_d^{BAY\prime}$. [c]From SPR (see the text). Values in the absence of NO were fit with a calculated R_{max}, and those in the presence of NO were fit with a floating R_{max}. Errors are from the fitting. NB means no binding. [d]From fitting of the Soret shift (1 cm cuvette). Values are means and the standard deviation of three to five independent measurements. For YC-1, 1 μM protein was used. For PF-25, both 1 and 0.5 μM protein was used. [e]From fitting of the Soret shift (1 and 10 cm cuvettes). Values are means and the standard deviation of 3–10 independent measurements. For YC-1 (10 measurements), measurements with protein concentrations of 0.1 μM (10 cm cuvette) and 0.5 and 1.0 μM (1 cm cuvette) were included. For BAY 41-2272 (three measurements), protein concentrations of 0.05 and 0.1 μM were included (10 cm cuvette). [f]From ref 32, measured in the presence of Mn^{2+}. [g]From ref 24, with an EC_{50} value for stimulating bovine sGC in the absence of NO or CO. [h]From ref 51, measured in the presence of GTP.

dx.doi.org/10.1021/bi4015133 | *Biochemistry* 2014, 53, 101–114

Table 3. Cooperativity Factors for sGC Proteins

	K_{int} (CO)[a]			$K_d^{CO}/K_d^{CO'}$			$K_d^{PF-25}/K_d^{PF-25'}$ (NO)
protein	YC-1	PF-25	BAY	YC-1	PF-25	BAY	PF-25
Ms sGC-NT13	19 ± 2	53 ± 3	NM[b]	19 ± 3	18 ± 2	212 ± 23	
Ms sGC-NT21	13.8 ± 0.3	19 ± 4	58 ± 7	11 ± 1	9 ± 1	31 ± 5	14 ± 3
Ms sGC β_1(1−380)							13 ± 2

[a]From global fitting. [b]Could not be readily measured by global fitting because of the large cooperativity factor, requiring that both 1 and 10 cm cuvettes be used.

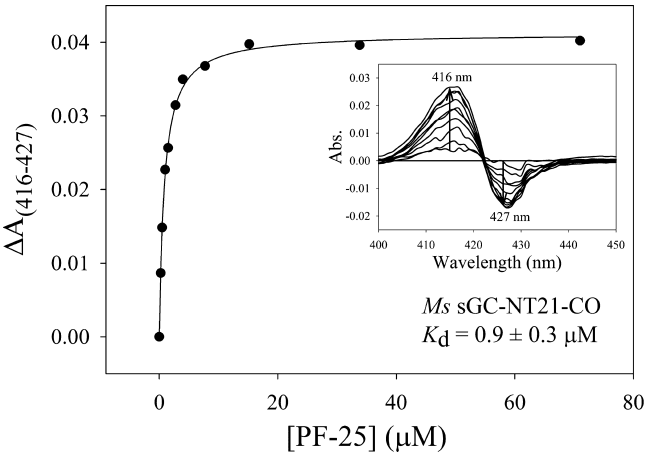

Figure 4. Binding of YC-1 to *Ms* sGC-NT-CO. Representative curve for binding of PF-25 to *Ms* sGC-NT21-CO. *Ms* sGC-NT-CO complexes were prepared in either 1 cm (1 μM protein, shown) or 10 cm (0.1 μM protein, BAY 41-2272) septum-capped cuvettes containing CO-saturated buffer [50 mM potassium phosphate (pH 7.4), 100 mM KCl, and 5% glycerol]. YC-1 family compounds (1 or 15 mM in ethanol) were titrated into the cuvettes, and the shift in the Soret band was monitored [$\Delta A_{(416-427)}$]. The data were fit to a single-site saturation model to obtain the dissociation constants for binding of the compound to the *Ms* sGC-NT-CO complex. The inset shows difference spectra upon compound titration. Ethanol or DMSO alone or other unrelated ring-containing compounds do not generate a shift in the Soret band (data not shown).

2). We examined binding of YC-1 to *Ms* sGC-NT21-CO and *Ms* sGC-NT13-CO in 10 and 1 cm cuvettes, respectively, which yielded values nearly identical to those obtained from the linked equilibrium analysis (Table 2). Likewise, estimating cooperativity factors by linked equilibrium analysis or by the ratio of K_d^{CO} to $K_d^{CO'}$ yielded similar values (Table 3), indicating good internal consistency between the two approaches. A shift in Soret band maxima was not observed for *Ms* sGC β_1(1−380).

Relative YC-1, BAY 41-2272, and PF-25 Binding Affinities. We examined binding by compounds BAY 41-2272, which is active at concentrations lower than those of YC-1,[22] and Pfizer compound 25 (PF-25), a recently described compound with greater aqueous solubility.[44] PF-25 behaves like other YC-1 family compounds, stimulating human sGC in the presence of NO (EC_{20} = 80 nM) and relaxing preconstricted aortic rings (IC_{50} = 60 nM). Both compounds are derived from YC-1 (Figure 1), differing mainly through substitution of the YC-1 furan ring. Affinity measurements were taken using linked equilibria and/or the Soret band shift. Interestingly, differences were observed among the compounds for binding to both the unliganded and CO-liganded proteins, and for their associated cooperativity factors. As with CO, YC-1 family compounds also bind tighter to *Ms* sGC-NT21 than to *Ms* sGC-NT13, indicating that the α_1 H-NOX domain not only interferes with CO binding but also interferes with YC-1 family compound binding (Table 2). The effect of H-NOX removal on stimulator binding is greater for BAY 41-2272 (~9-fold) than for YC-1 or PF-25 (~2-fold).

Binding of stimulator compounds to the CO complexes is much tighter than binding to the unliganded proteins. The greatest enhancement is seen for BAY 41-2272, which binds to the CO complex with a K_d of 30−90 nM, whereas YC-1 binds with a K_d of ~1 μM and PF-25 with a K_d of ~3 μM (Table 2). PF-25 binds particularly poorly to the unliganded proteins (70−150 μM).

Measuring PF-25 Binding Using Surface Plasmon Resonance. We hypothesized that YC-1 family compounds bind to the α_1 PAS domain because (i) PAS domains commonly bind small molecules in their capacity as signaling proteins,[11] (ii) the α_1 PAS domain is required for observing a YC-1-dependent enhancement in CO affinity (Table 1), and (iii) addition of YC-1 did not lead to a shift in the Soret absorption band for any of the proteins lacking the α chain. To directly address whether YC-1 binds to the α_1 PAS domain, we used surface plasmon resonance (SPR), allowing for binding measurements that were not dependent on heme spectra. To accomplish this, we specifically biotinylated *Ms* sGC NT21, α_1 PAS, and β_1(1−380) at their C-termini, using biotin ligase (BirA) and sGC proteins modified to contain the BirA recognition sequence.[52] The biotinylated proteins were captured in the SPR instrument on a NeutrAvidin-coated sensor chip, and analyte binding was examined. Unfortunately, neither YC-1 nor BAY 41-2272 was suitable for SPR binding measurements because of their poor solubility in aqueous buffer. Introducing these compounds required a percentage of DMSO greater than the percentage that was well tolerated by the protein over the course of the measurements, which take hours to complete. We therefore turned to PF-25, a compound better suited to SPR measurements because of its greater aqueous solubility.

Binding of PF-25 to *Ms* sGC NT21 was clearly observed in the SPR instrument (Figure 5). Binding was rapid, as expected from our CO titration experiments, making k_{on} measurements unreliable. Release was also rapid and difficult to quantify. Ligand affinity was therefore estimated through saturation binding, leading to a K_d^{PF-25} of 153 μM, a value similar to that observed through analysis by linked equilibria. Unexpectedly, binding to *Ms* sGC β_1(1−380) was also observed (K_d^{PF-25} = 92 μM). In contrast, binding to *Ms* sGC α_1 PAS was not observed. Thus, these data indicated PF-25 binds to the β_1 chain between residues 1 and 380.

Measuring binding of PF-25 to the CO-saturated protein was not possible because the SPR instrument has an in-line degasser to prevent bubble formation. We therefore examined binding after addition of NO to the heme-containing constructs, which could be saturated with small amounts of NO released *in situ*. Unlike with CO, only nanomolar concentrations of NO were

dx.doi.org/10.1021/bi4015133 | *Biochemistry* 2014, 53, 101−114

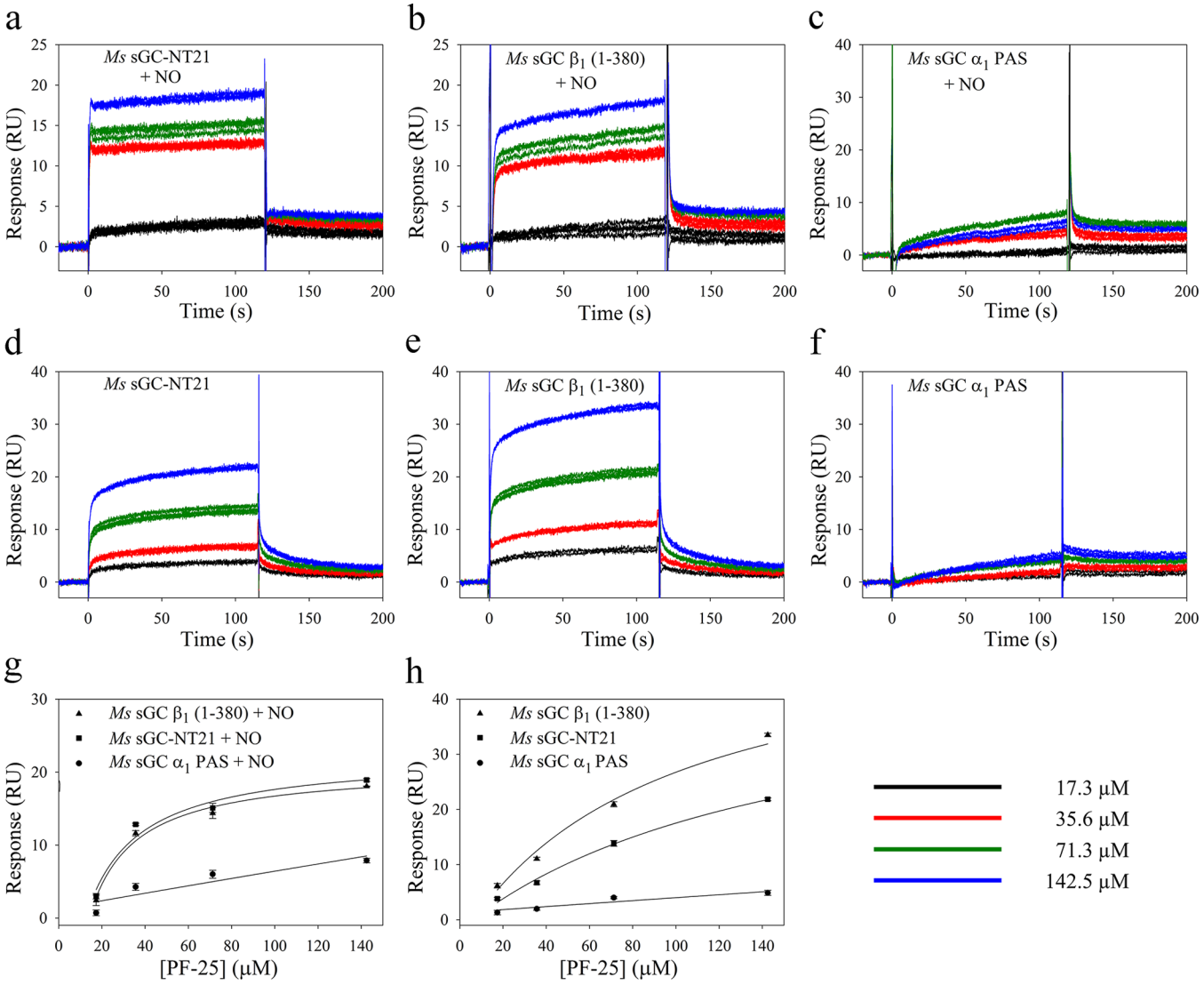

Figure 5. Binding of PF-25 to *Ms* sGC constructs examined by surface plasmon resonance. Biotinylated *Ms* sGC-NT21, *Ms* sGC α_1 PAS, and *Ms* sGC β_1(1−380) were captured on an SPR chip containing immobilized NeutrAvidin. Solutions of PF-25 with or without DEA/NO were injected into the chip, and the response change was recorded. The injected samples contained 50 mM potassium phosphate buffer (pH 7.4), 100 mM KCl, 2 mM EDTA, 1 mM TCEP, 1% DMSO, PF-25 (0−142.5 μM), and, where included, 25 μM DEA/NO. Shown are representative sensorgrams for PF-25 binding in the presence (a−c) and absence (d−f) of DEA/NO. Three trials are shown for each PF-25 concentration. Binding data were analyzed with the Biacore T-100 evaluation software. Values for K_d were obtained using a single-site saturation model (SigmaPlot) by plotting the response (RU) with respect to PF-25 concentration using a floating R_{max} (g) or a calculated R_{max} (h).

required for these measurements because of the high affinity of NO for sGC heme (picomolar to nanomolar) and the small amount of protein captured on the chip surface (picomoles). Binding of NO to heme enhanced binding of PF-25 to *Ms* sGC NT21 as expected ($K_d^{PF\text{-}25\prime}$ = 11 μM) but, in contrast to CO, also enhanced binding of PF-25 to *Ms* sGC β_1(1−380) (Figure 5 and Table 2), yielding a $K_d^{PF\text{-}25\prime}$ of 7 μM. Surprisingly, PF-25 also bound slightly weaker to *Ms* sGC-NT21-NO than to *Ms* sGC-NT21-CO. The reason for these differences in binding is not yet clear but is presumably due to differences in the conformations of the NO and CO complexes.

Binding of YC-1 to *Ms* sGC PAS Domains Is Not Observed by Fluorescence Anisotropy. We examined binding of YC-1 to PAS domains in solution using fluorescence anisotropy. Various proteins were titrated into a YC-1-containing solution, and changes in YC-1-dependent fluorescence anisotropy were monitored. Weak binding (>100 μM) was indicated for *Ms* sGC α_1 PAS, but not for lysozyme. However, the data were extremely noisy, nonsaturable, and slow to equilibrate, suggesting the observed interaction was nonspecific. Likewise, a weak signal was also seen for the β_1 PAS domain, although it was less substantial, and also likely to be due to nonspecificity. Binding to heme-containing *Ms* sGC proteins could not be measured because of signal quenching by the heme. Although inconclusive, these data indicate the individual sGC PAS domains do not contain the YC-1 binding site, consistent with our SPR data.

DISCUSSION

YC-1 family compounds show great promise for the treatment of cardiovascular disease through their stimulation of sGC, yet their mechanism of action remains unknown. Likewise, the mechanism by which binding of NO to sGC heme stimulates cyclase activity is unclear. Here, we show that (i) the α_1 PAS

dx.doi.org/10.1021/bi4015133 | *Biochemistry* 2014, 53, 101−114

domain inhibits binding of CO, and presumably NO, to the β_1 heme domain, (ii) binding of YC-1 overcomes this inhibition, (iii) binding of YC-1 and CO or NO to heterodimeric sGC displays linked equilibria, with binding of one enhancing binding of the other, (iv) monomeric β_1 sGC displays high CO affinity and loss of CO−YC-1 linked equilibria, and (v) YC-1 binds to the β_1 chain, most likely in the heme domain. A model emerges from our study in which the α_1 H-NOX and PAS domains act to inhibit the β_1 H-NOX domain, which, in turn, acts to inhibit the cyclase domain. Activation of cyclase can occur through the relieving of either inhibitory contact; maximal activity occurs when both inhibitory contacts are removed. In what follows, we expand upon these findings.

YC-1 Binding to or near the sGC Heme Domain. Discovery of the YC-1 binding site has been challenging because of the difficulty in working with sGC protein. Suggestions in the literature for where YC-1 binds invoke nearly all sGC domains, including the α_1 H-NOX domain,[33,34,53] the catalytic domain,[31,32,54] and the heme domain.[35−38,55,56] Here, using SPR, we demonstrate that binding is to the N-terminal portion of the β_1 chain. Because binding to the β_1 PAS domain could not be detected by fluorescence anisotropy measurements, binding is most likely to the heme-containing β_1 H-NOX domain. Additionally, a recent report notes that a human sGC construct lacking both H-NOX domains is not stimulated by BAY 41-2272, while full-length sGC is.[57]

Binding of YC-1 leads to an ∼2 nm shift in the Soret absorption band for the CO complex,[38,41,55] which we used to determine the YC-1 dissociation constants to be 0.8 and 0.6 μM for *Ms* sGC-NT13-CO and *Ms* sGC NT21-CO, respectively (Figure 4 and Table 2). Others have used this shift in absorbance,[38,55] or a shift in the Raman heme spectrum upon addition of YC-1 or BAY 41-2272,[35−37,56,58] to argue that YC-1 family compounds bind to the heme domain. However, the high concentrations of YC-1 used in those studies (generally 200 μM) raise the concern that the spectral changes may have arisen from nonspecific binding. Here, we demonstrate that only nanomolar quantities of YC-1 are required for inducing the shift in the *Ms* sGC-NT-CO Soret absorption band, consistent with a specific binding event.

YC-1 readily enhances CO binding in *Ms* sGC-NT proteins (Table 1 and ref 33), which lack the cyclase domain, but does not stimulate the isolated cyclase domains.[59] YC-1 also readily enhances binding of CO to *Ms* sGC-NT21 (Table 1 and ref 43), which does not contain the α_1 H-NOX domain, ruling out the possibility of the α_1 H-NOX domain containing the binding site. A similar conclusion was reached for truncated versions of mammalian sGC proteins.[48−50] These data, taken together with our SPR and spectral data, provide a compelling argument for heme domain binding of YC-1 family compounds.

Results using the bovine protein are qualitatively the same as those for the *Manduca* protein but differ in the dissociation constants for CO binding. *Bt* sGC β_1(1−197) binds CO ∼8-fold less tightly than *Ms* sGC β_1(1−380) (Table 1), while binding by *Bt* sGC β_1(1−359) is weaker yet, ∼9-fold weaker than binding by *Bt* sGC β_1(1−197). Neither bovine protein displays a significant response to YC-1. The difference in CO affinity between *Bt* sGC β_1(1−197) and *Bt* sGC β_1(1−359) may result from stabilization of the lower-affinity form of the H-NOX domain upon homodimer formation in the larger protein or from interactions between the H-NOX and PAS domains.

YC-1 Binding Relieves Inhibition of the β_1 Heme Domain by the α_1 H-NOX and PAS Domains. Perhaps our most unexpected finding is that the affinity of CO for heme in the β_1 H-NOX domain is as high in the absence of other domains as it is in the presence of YC-1 (Table 1). We showed previously that YC-1 binding leads to tighter CO binding in *Ms* sGC-NT constructs[33] and that binding leads to the development of a geminate recombination phase upon CO photolysis.[41] Negrerie and co-workers recently showed that the isolated human H-NOX domain [β_1(1−190)] also displays a geminate rebinding phase whereas the full-length protein does not.[60] This tighter binding and trapped CO correlate with increased cyclase activity for full-length sGC proteins.[25,61] We now show that both the α_1 PAS and α_1 H-NOX domains impair CO binding (Table 1). Removal of the α_1 H-NOX domain enhances CO binding by 24-fold, and complete removal of the α_1 chain enhances CO binding by 265-fold (Table 1). Binding of CO to *Ms* sGC β_1(1−380) in the absence of YC-1 is as tight (K_d^{CO} = 0.20 μM) as binding to any of the *Ms* sGC-NT proteins in the presence of YC-1. Cooperativity in binding of CO to any of the constructs missing the α_1 chain is now largely absent (K_{int} ∼ 1), and YC-1 binding does not appreciably enhance CO binding (Table 1). In addition to tightly binding CO, *Ms* sGC β_1(1−380) presumably also binds tightly to YC-1 and BAY 41-2272.

The situation with NO binding is similar to that for CO but apparently differs with respect to cooperativity. Unlike CO binding, NO binding leads to proximal histidine cleavage and a five-coordinate Fe−NO complex. NO release is multiphasic. We previously showed that binding of YC-1 to *Ms* sGC-NT-NO eliminated the faster of two NO release rates, yielding a protein with higher NO affinity, much like what occurs with CO.[33] However, unlike with CO, the data in Table 2 indicate that binding of NO enhances binding of PF-25 to *Ms* sGC β_1(1−380) by ∼10-fold, indicating that cooperativity occurs for NO with this protein but not for CO. The reason for this difference is unclear but may have to do with the difference in heme domain conformation for the five-coordinate and six-coordinate *Ms* sGC proteins.

We recently determined the crystal structure of *Ms* sGC α_1 PAS[17] and a molecular model for domain packing based on homology modeling, chemical cross-linking, and SAXS analysis.[43] These data indicate a direct contact between one face of helix Fα in *Ms* sGC α_1 PAS, involving residues Glu 340 and Lys 343, and the subdomain containing proximal His 105 that is proposed to be involved in signal transduction[62−64] (Figure 6). This contact in the intact protein may serve to stabilize the H-NOX domain in a low-affinity conformation. A pocket in this subdomain identified in our homology model may be the YC-1 binding site and provide a means for counteracting the effects of α_1 PAS inhibition. Our cross-linking data also indicate direct contact between the α_1 and β_1 H-NOX domains (Figure 6). This contact is farther from the heme and may serve to enhance the α_1 PAS−β_1 H-NOX interaction.

Binding Affinity of YC-1 Family Compounds. Just as YC-1 binding enhances binding of CO to heterodimeric sGC, CO binding enhances YC-1 binding, highlighting both the allosteric nature of sGC and the linked equilibria between CO and YC-1 binding events. Binding to *Ms* sGC-NT13 in the absence of CO (Figure 3 and Table 2) varies from ∼20 μM for YC-1 and BAY 41-2272 to 155 μM for PF-25. Binding to *Ms* sGC-NT21 is slightly tighter than to *Ms* sGC-NT13, particularly for BAY 41-2272, indicating that the α_1 H-NOX

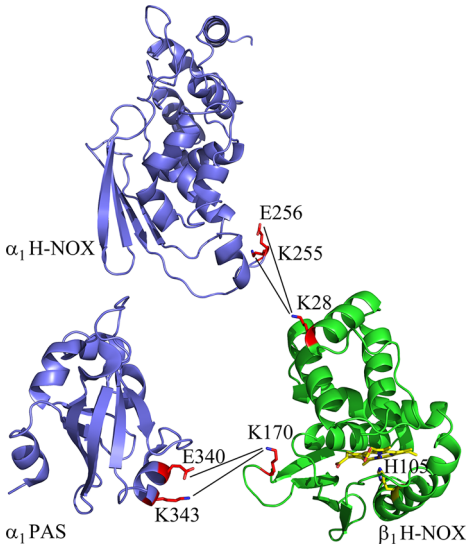

Figure 6. Contact residues of α_1 H-NOX, α_1 PAS, and β_1 H-NOX domains. Shown is the crystal structure for the α_1 PAS domain (Protein Data Bank entry 4GJ4[17]) and homology models for the α_1 and β_1 H-NOX domains. Cross-links between the two domains identified by mass spectrometry are shown,[43] as are the heme and proximal histidine in the β_1 H-NOX domain. This figure was prepared using PyMOL (W. L. DeLano, http://www.pymol.org).

domain inhibits not only CO binding but also binding by stimulator compounds.

Binding of YC-1 family compounds to *Ms* sGC-NT-CO complexes is 10−200-fold tighter than that to *Ms* sGC-NT (Figure 4 and Tables 2 and 3). BAY 41-2272 binds particularly tightly to the CO complexes, displaying dissociation constants of 30−90 nM. Thus, the enhanced stimulation of sGC by BAY 41-2272 as compared to that with other YC-1 family compounds appears to be due to especially tight binding to the active conformation.

Binding of PF-25 to the *Ms* sGC-NT21-NO complex, examined using SPR, was ∼2-fold weaker than binding to the *Ms* sGC β_1(1−380)-NO complex, consistent with the unliganded and CO-bound binding studies (Table 2), and consistent with a model in which the α_1 PAS domain inhibits binding of CO, NO, or YC-1 family compounds. Interestingly, binding of PF-25 to the *Ms* sGC-NT21-NO complex is 3−12-fold weaker than binding to the *Ms* sGC-NT21-CO complex.

The YC-1 dissociation constants we measure for the unliganded and truncated *Ms* sGC proteins are similar to those reported for binding and stimulating the full-length protein. Binding to full-length bovine lung sGC was monitored using equilibrium dialysis, yielding a K_d of 52 μM when measured in the presence of Mn^{2+},[32] and by the effective concentration needed to achieve 50% maximal stimulation of unliganded bovine sGC, yielding an EC_{50} of ∼20 μM.[24] These values compare favorably with those of a stimulator binding to *Ms* sGC-NT13 ($K_d^{YC\text{-}1}$ = 21 μM). Additionally, similar concentrations are needed for BAY 41-2272 to bind *Ms* sGC-NT21-CO ($K_d^{BAY'}$ = 0.09 μM) and for BAY 41-2272 to stimulate sGC in preconstricted aortic rings (EC_{50} = 0.3 μM[34]). This agreement between binding affinity for *Ms* sGC-NT and the concentration needed to stimulate activity in the full-length protein provides confidence that our measurements reflect the functionally important binding events.

A Model for sGC Regulation. The model that emerges from our data is one in which the low-energy state for the heme pocket differs between the isolated β_1 H-NOX domain and heterodimeric sGC (Figure 7). In the isolated domain, the heme pocket traps CO and NO, leading to high affinity for these ligands. In heterodimeric sGC, the heme pocket changes conformation such that NO and CO can more readily escape and binding affinity is reduced. Binding of YC-1 family compounds to heterodimeric sGC alters or severs the connection between the heme domain and α_1 subunit, returning the heme domain to its high-affinity conformation. A prediction of this model is that CO or NO binding will induce the high-affinity heme domain conformation, leading to tighter binding by YC-1 family compounds. Linked equilibria were in fact observed: YC-1 family compounds bind 10−200-fold more tightly in the presence of CO or NO than in their absence (Table 2).

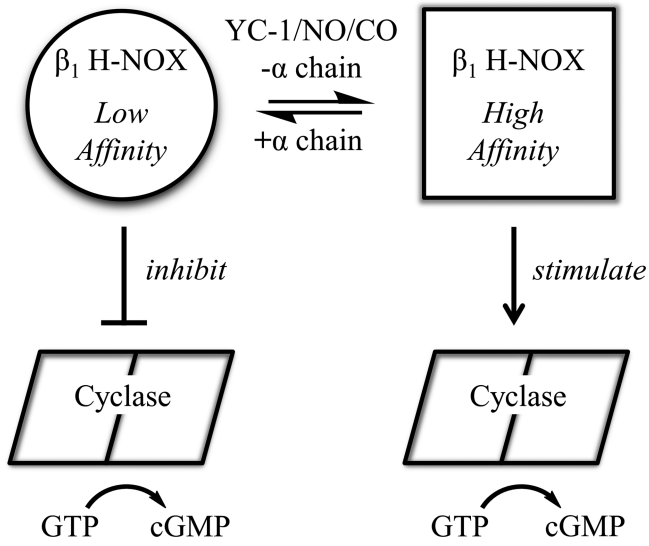

Figure 7. Model for sGC regulation. Shown is a proposed model for allosteric regulation in sGC in which the β_1 H-NOX is in equilibrium between high- and low-affinity conformations. YC-1, NO, CO, and the absence of α_1 chain H-NOX and PAS domains all shift the equilibria toward high affinity, while the α_1 chain H-NOX and PAS domains shift the equilibria toward low affinity. The low-affinity conformer is inhibitory toward the cyclase domains, while the high-affinity conformer is noninhibitory or possibly stimulatory.

A second prediction of this model is that the low-affinity H-NOX conformation inhibits cyclase activity, while the high-affinity conformation relieves this inhibition or is stimulatory. In this way, binding of either YC-1 or CO/NO leads to cyclase activation, and binding of both yields full sGC activation. Support for this model comes from studies of sGC mutant β_1H105C, in which the heme proximal histidine is mutated to cysteine, leading to heme-free sGC and a presumably high-affinity conformation for the H-NOX domain. This protein displays high basal catalytic activity and can still be stimulated by YC-1.[65,66] Additional support for the model comes from studies of the rat cyclase domain alone and after addition of the H-NOX domain in trans, which leads to inhibition of cyclase activity[67] and protection of cyclase from hydrogen−deuterium exchange.[64] Although inhibition was insensitive to NO, these data support a model in which the H-NOX domain directly binds to and inhibits the cyclase domain.[67] The possibility that

dx.doi.org/10.1021/bi4015133 | *Biochemistry* 2014, 53, 101−114

the high-affinity heme domain conformation may in fact stimulate cyclase activity rather than simply remove an inhibitory contact is suggested by experiments with sGC lacking both H-NOX domains, which displays only basal catalytic activity.[57] Interestingly, this protein is also insensitive to BAY 41−2272.

A third prediction of this model is that linked equilibria should exist between nucleotide binding to the cyclase domain and ligand binding to the heme domain. The fact that such a link exists has been previously described.[68−70] In the presence of nucleotide, NO release is slowed,[69] full stimulation by NO enhanced,[68] and desensitization delayed.[70]

How the β_1 H-NOX domain switches from low to high CO and NO affinity is unknown. One recently proposed possibility is that the proximal heme pocket is strained in the low-affinity form, leading to heme distortion and inherently poor CO and NO binding affinity. Upon bond breakage, CO and NO escape rather than re-bind to heme.[38,60,71,72] In the high-affinity state, proximal strain is relieved by movement of the proximal histidine and heme iron into the plane of the porphyrin ring, yielding greater CO or NO affinity and a higher capture rate.[72] This model is reminiscent of the "relaxed" and "tense" states described for hemoglobin.

A second possibility is for the heme domain to adopt "open" and "closed" conformations, in which the closed conformation hinders the escape of CO or NO and favors capture by heme. This is the strategy employed by *Rhodnius prolixus* nitrophorin 4, an NO transport protein. In nitrophorin 4, two loops collapse into the heme pocket at low pH, generating a closed conformation, an increased level of geminate recombination, and a higher affinity for NO.[73−75] Distinguishing between these models awaits determination of high-resolution structures.

AUTHOR INFORMATION

Corresponding Author

*Department of Chemistry and Biochemistry, The University of Arizona, 1041 E. Lowell St., Tucson, AZ 85721. E-mail: montfort@email.arizona.edu. Telephone: (520) 621-1884. Fax: (520) 626-9204.

Funding

This work was supported in part by grants from the National Institutes of Health (HL062969 to W.R.M. and U54 CA143924 to W.R.M. and M.J.G.) and the American Heart Association (11PRE7610113 to R.P. and 10SDG2600345 to E.D.G.).

Notes

The authors declare no competing financial interest.

ACKNOWLEDGMENTS

We thank Alex Hailey and Scott Ogley for help with evaluating expression of PAS domains containing differing C-termini. We are grateful to Jacquie Brailey for help with protein expression and to Dr. Patrick Loll for providing us with his SUMO fusion ligation-independent cloning vector. We thank Dr. Lee Roberts for Pfizer compound PF-25 and Dr. Katrina Miranda for DEA/NO. SPR data were acquired by the Arizona Proteomics Consortium supported by National Institute of Environmental Health Sciences Grant ES06694 to the Southwest Environmental Health Sciences Center, National Cancer Institute Grant CA023074 to the Arizona Cancer Center, and the BIO5 Institute of The University of Arizona. The Biacore T100 biosensor was provided though generous support of the Prescott Friends of the Sarver Heart Center with leadership gifts from Jim and Linda Lee, Ron and Laura James, and Swayze and Kathy McCraine.

ABBREVIATIONS

sGC, soluble guanylyl cyclase; *Ms* sGC, *M. sexta* sGC; *Bt* sGC, *Bos taurus* (bovine) sGC; DEA/NO, 2-(*N*,*N*-diethylamino)-diazenolate 2-oxide; CC, coiled coil; PAS, Per-ARNT-Sim; H-NOX, heme-nitric oxide/oxygen binding; SPR, surface plasmon resonance; SAXS, small-angle X-ray scattering.

REFERENCES

(1) Ignarro, L. J., Ed. (2010) *Nitric Oxide Biology and Pathobiology*, 2nd ed., Academic Press, San Diego.

(2) Bian, K., Doursout, M. F., and Murad, F. (2008) Vascular system: Role of nitric oxide in cardiovascular diseases. *J. Clin. Hypertens. (Hoboken, NJ, U.S.) 10*, 304−310.

(3) Coggins, M. P., and Bloch, K. D. (2007) Nitric oxide in the pulmonary vasculature. *Arterioscler., Thromb., Vasc. Biol. 27*, 1877−1885.

(4) Li, H., and Poulos, T. L. (2005) Structure-function studies on nitric oxide synthases. *J. Inorg. Biochem. 99*, 293−305.

(5) Stuehr, D. J., Tejero, J., and Haque, M. M. (2009) Structural and mechanistic aspects of flavoproteins: Electron transfer through the nitric oxide synthase flavoprotein domain. *FEBS J. 276*, 3959−3974.

(6) Brunton, T. L. (1867) Use of Nitrite of Amyl in Angina Pectoris. *Lancet 90*, 97−98.

(7) Murrell, W. (1879) Nitro-glycerine as a remedy for angina pectoris. *Lancet 113*, 113−115.

(8) Derbyshire, E. R., and Marletta, M. A. (2012) Structure and regulation of soluble guanylate cyclase. *Annu. Rev. Biochem. 81*, 533−559.

(9) Cary, S. P., Winger, J. A., Derbyshire, E. R., and Marletta, M. A. (2006) Nitric oxide signaling: No longer simply on or off. *Trends Biochem. Sci. 31*, 231−239.

(10) Nioche, P., Berka, V., Vipond, J., Minton, N., Tsai, A. L., and Raman, C. S. (2004) Femtomolar sensitivity of a NO sensor from *Clostridium botulinum*. *Science 306*, 1550−1553.

(11) Moglich, A., Ayers, R. A., and Moffat, K. (2009) Structure and signaling mechanism of Per-ARNT-Sim domains. *Structure 17*, 1282−1294.

(12) Liu, Y., Ruoho, A. E., Rao, V. D., and Hurley, J. H. (1997) Catalytic mechanism of the adenylyl and guanylyl cyclases: Modeling and mutational analysis. *Proc. Natl. Acad. Sci. U.S.A. 94*, 13414−13419.

(13) Dierks, E. A., Hu, S., Vogel, K. M., Yu, A. E., Spiro, T. G., and Burstyn, J. N. (1997) Demonstration of the role of scission of the proximal histidine-iron bond in the activation of soluble guanylyl cyclase though metalloporphyrin substitution studies. *J. Am. Chem. Soc. 119*, 7316−7323.

(14) Stone, J. R., and Marletta, M. A. (1996) Spectral and kinetic studies on the activation of soluble guanylate cyclase by nitric oxide. *Biochemistry 35*, 1093−1099.

(15) Wedel, B., Humbert, P., Harteneck, C., Foerster, J., Malkewitz, J., Böhme, E., Schultz, G., and Koesling, D. (1994) Mutation of His-105 in the β1 subunit yields a nitric oxide-insensitive form of soluble guanylate cyclase. *Proc. Natl. Acad. Sci. U.S.A. 91*, 2592−2596.

(16) Ma, X., Beuve, A., and van den Akker, F. (2010) Crystal structure of the signaling helix coiled-coil domain of the β1 subunit of the soluble guanylyl cyclase. *BMC Struct. Biol. 10*, 2.

(17) Purohit, R., Weichsel, A., and Montfort, W. R. (2013) Crystal structure of the α subunit PAS domain from soluble guanylyl cyclase. *Protein Sci. 22*, 1439−1444.

(18) Allerston, C. K., von Delft, F., and Gileadi, O. (2013) Crystal structures of the catalytic domain of human soluble guanylate cyclase. *PLoS One 8*, e57644.

(19) Pellicena, P., Karow, D. S., Boon, E. M., Marletta, M. A., and Kuriyan, J. (2004) Crystal structure of an oxygen-binding heme domain related to soluble guanylate cyclases. *Proc. Natl. Acad. Sci. U.S.A. 101*, 12854−12859.

(20) Ma, X., Sayed, N., Baskaran, P., Beuve, A., and van den Akker, F. (2008) PAS-mediated Dimerization of Soluble Guanylyl Cyclase Revealed by Signal Transduction Histidine Kinase Domain Crystal Structure. *J. Biol. Chem. 283*, 1167−1178.
(21) Ma, X., Sayed, N., Beuve, A., and van den Akker, F. (2007) NO and CO differentially activate soluble guanylyl cyclase via a heme pivot-bend mechanism. *EMBO J. 26*, 578−588.
(22) Evgenov, O. V., Pacher, P., Schmidt, P. M., Hasko, G., Schmidt, H. H., and Stasch, J. P. (2006) NO-independent stimulators and activators of soluble guanylate cyclase: Discovery and therapeutic potential. *Nat. Rev. Drug Discovery 5*, 755−768.
(23) Ko, F. N., Wu, C. C., Kuo, S. C., Lee, F. Y., and Teng, C. M. (1994) YC-1, a novel activator of platelet guanylate cyclase. *Blood 84*, 4226−4233.
(24) Friebe, A., Schultz, G., and Koesling, D. (1996) Sensitizing soluble guanylyl cyclase to become a highly CO-sensitive enzyme. *EMBO J. 15*, 6863−6868.
(25) Stone, J. R., and Marletta, M. A. (1998) Synergistic activation of soluble guanylate cyclase by YC-1 and carbon monoxide: Implications for the role of cleavage of the iron-histidine bond during activation by nitric oxide. *Chem. Biol. 5*, 255−261.
(26) Ramanathan, S., Mazzalupo, S., Boitano, S., and Montfort, W. R. (2011) Thrombospondin-1 and angiotensin II inhibit soluble guanylyl cyclase through an increase in intracellular calcium concentration. *Biochemistry 50*, 7787−7799.
(27) Belik, J. (2009) Riociguat, an oral soluble guanylate cyclase stimulator for the treatment of pulmonary hypertension. *Curr. Opin. Invest. Drugs 10*, 971−979.
(28) Mittendorf, J., Weigand, S., Alonso-Alija, C., Bischoff, E., Feurer, A., Gerisch, M., Kern, A., Knorr, A., Lang, D., Muenter, K., Radtke, M., Schirok, H., Schlemmer, K. H., Stahl, E., Straub, A., Wunder, F., and Stasch, J. P. (2009) Discovery of riociguat (BAY 63-2521): A potent, oral stimulator of soluble guanylate cyclase for the treatment of pulmonary hypertension. *ChemMedChem 4*, 853−865.
(29) Ghofrani, H. A., Galie, N., Grimminger, F., Grunig, E., Humbert, M., Jing, Z. C., Keogh, A. M., Langleben, D., Kilama, M. O., Fritsch, A., Neuser, D., and Rubin, L. J. (2013) Riociguat for the treatment of pulmonary arterial hypertension. *N. Engl. J. Med. 369*, 330−340.
(30) Ghofrani, H. A., D'Armini, A. M., Grimminger, F., Hoeper, M. M., Jansa, P., Kim, N. H., Mayer, E., Simonneau, G., Wilkins, M. R., Fritsch, A., Neuser, D., Weimann, G., and Wang, C. (2013) Riociguat for the treatment of chronic thromboembolic pulmonary hypertension. *N. Engl. J. Med. 369*, 319−329.
(31) Lamothe, M., Chang, F. J., Balashova, N., Shirokov, R., and Beuve, A. (2004) Functional characterization of nitric oxide and YC-1 activation of soluble guanylyl cyclase: Structural implication for the YC-1 binding site? *Biochemistry 43*, 3039−3048.
(32) Yazawa, S., Tsuchiya, H., Hori, H., and Makino, R. (2006) Functional characterization of two nucleotide-binding sites in soluble guanylate cyclase. *J. Biol. Chem. 281*, 21763−21770.
(33) Hu, X., Murata, L. B., Weichsel, A., Brailey, J. L., Roberts, S. A., Nighorn, A., and Montfort, W. R. (2008) Allostery in recombinant soluble guanylyl cyclase from *Manduca sexta*. *J. Biol. Chem. 283*, 20968−20977.
(34) Stasch, J.-P., Becker, E. M., Alonso-Alija, C., Apeler, H., Gerzer, R., Minuth, T., Perzborn, E., Pleiss, U., Schröder, H., Schroeder, W., Stahl, E., Steinke, W., Straub, A., and Schramm, M. (2001) NO-independent regulatory site on soluble guanylate cyclase. *Nature 410*, 212−215.
(35) Ibrahim, M., Derbyshire, E. R., Marletta, M. A., and Spiro, T. G. (2010) Probing soluble guanylate cyclase activation by CO and YC-1 using resonance Raman spectroscopy. *Biochemistry 49*, 3815−3823.
(36) Ibrahim, M., Derbyshire, E. R., Soldatova, A. V., Marletta, M. A., and Spiro, T. G. (2010) Soluble guanylate cyclase is activated differently by excess NO and by YC-1: Resonance Raman spectroscopic evidence. *Biochemistry 49*, 4864−4871.
(37) Martin, E., Czarnecki, K., Jayaraman, V., Murad, F., and Kincaid, J. (2005) Resonance Raman and infrared spectroscopic studies of high-output forms of human soluble guanylyl cyclase. *J. Am. Chem. Soc. 127*, 4625−4631.
(38) Yoo, B. K., Lamarre, I., Rappaport, F., Nioche, P., Raman, C. S., Martin, J. L., and Negrerie, M. (2012) Picosecond to second dynamics reveals a structural transition in *Clostridium botulinum* NO-sensor triggered by the activator BAY-41-2272. *ACS Chem. Biol. 7*, 2046−2054.
(39) Schmidt, P. M., Schramm, M., Schroder, H., Wunder, F., and Stasch, J. P. (2004) Identification of residues crucially involved in the binding of the heme moiety of soluble guanylate cyclase. *J. Biol. Chem. 279*, 3025−3032.
(40) Schindler, U., Strobel, H., Schonafinger, K., Linz, W., Lohn, M., Martorana, P. A., Rutten, H., Schindler, P. W., Busch, A. E., Sohn, M., Topfer, A., Pistorius, A., Jannek, C., and Mulsch, A. (2006) Biochemistry and pharmacology of novel anthranilic acid derivatives activating heme-oxidized soluble guanylyl cyclase. *Mol. Pharmacol. 69*, 1260−1268.
(41) Hu, X., Feng, C., Hazzard, J. T., Tollin, G., and Montfort, W. R. (2008) Binding of YC-1 or BAY 41-2272 to Soluble Guanylyl Cyclase Induces a Geminate Phase in CO Photolysis. *J. Am. Chem. Soc. 130*, 15748−15749.
(42) Fritz, B. G., Hu, X., Brailey, J. L., Berry, R. E., Walker, F. A., and Montfort, W. R. (2011) Oxidation and loss of heme in soluble guanylyl cyclase from *Manduca sexta*. *Biochemistry 50*, 5813−5815.
(43) Fritz, B. G., Roberts, S. A., Ahmed, A., Breci, L., Li, W., Weichsel, A., Brailey, J. L., Wysocki, V. H., Tama, F., and Montfort, W. R. (2013) Molecular Model of a Soluble Guanylyl Cyclase Fragment Determined by Small-Angle X-ray Scattering and Chemical Cross-Linking. *Biochemistry 52*, 1568−1582.
(44) Roberts, L. R., Bradley, P. A., Bunnage, M. E., England, K. S., Fairman, D., Fobian, Y. M., Fox, D. N., Gymer, G. E., Heasley, S. E., Molette, J., Smith, G. L., Schmidt, M. A., Tones, M. A., and Dack, K. N. (2011) Acidic triazoles as soluble guanylate cyclase stimulators. *Bioorg. Med. Chem. Lett. 21*, 6515−6518.
(45) Weeks, S. D., Drinker, M., and Loll, P. J. (2007) Ligation independent cloning vectors for expression of SUMO fusions. *Protein Expression Purif. 53*, 40−50.
(46) Liu, H., and Naismith, J. H. (2008) An efficient one-step site-directed deletion, insertion, single and multiple-site plasmid mutagenesis protocol. *BMC Biotechnol. 8*, 91.
(47) Kapust, R. B., Tozser, J., Fox, J. D., Anderson, D. E., Cherry, S., Copeland, T. D., and Waugh, D. S. (2001) Tobacco etch virus protease: Mechanism of autolysis and rational design of stable mutants with wild-type catalytic proficiency. *Protein Eng. 14*, 993−1000.
(48) Koglin, M., and Behrends, S. (2003) A functional domain of the α1 subunit of soluble guanylyl cyclase is necessary for activation of the enzyme by nitric oxide and YC-1 but is not involved in heme binding. *J. Biol. Chem. 278*, 12590−12597.
(49) Kraehling, J. R., Busker, M., Haase, T., Haase, N., Koglin, M., Linnenbaum, M., and Behrends, S. (2011) The amino-terminus of nitric oxide sensitive guanylyl cyclase α_1 does not affect dimerization but influences subcellular localization. *PLoS One 6*, e25772.
(50) Sharina, I. G., Jelen, F., Bogatenkova, E. P., Thomas, A., Martin, E., and Murad, F. (2008) α1 soluble guanylyl cyclase (sGC) splice forms as potential regulators of human sGC activity. *J. Biol. Chem. 283*, 15104−15113.
(51) Kharitonov, V. G., Sharma, V. S., Magde, D., and Koesling, D. (1999) Kinetics and equilibria of soluble guanylate cyclase ligation by CO: Effect of YC-1. *Biochemistry 38*, 10699−10706.
(52) Chen, I., Howarth, M., Lin, W., and Ting, A. Y. (2005) Site-specific labeling of cell surface proteins with biophysical probes using biotin ligase. *Nat. Methods 2*, 99−104.
(53) Pal, B., and Kitagawa, T. (2010) Binding of YC-1/BAY 41-2272 to soluble guanylate cyclase: A new perspective to the mechanism of activation. *Biochem. Biophys. Res. Commun. 397*, 375−379.
(54) Makino, R., Yazawa, S., Hori, H., and Shiro, Y. (2012) Interactions of soluble guanylate cyclase with a P-site inhibitor: Effects of gaseous heme ligands, azide, and allosteric activators on the binding of 2′-deoxy-3′-GMP. *Biochemistry 51*, 9277−9289.

(55) Sharma, V. S., and Magde, D. (1999) Activation of soluble guanylate cyclase by carbon monoxide and nitric oxide: A mechanistic model. *Methods 19*, 494−505.
(56) Li, Z., Pal, B., Takenaka, S., Tsuyama, S., and Kitagawa, T. (2005) Resonance Raman evidence for the presence of two heme pocket conformations with varied activities in CO-bound bovine soluble guanylate cyclase and their conversion. *Biochemistry 44*, 939−946.
(57) Sharina, I., Sobolevsky, M., Doursout, M. F., Gryko, D., and Martin, E. (2012) Cobinamides are novel coactivators of nitric oxide receptor that target soluble guanylyl cyclase catalytic domain. *J. Pharmacol. Exp. Ther. 340*, 723−732.
(58) Denninger, J. W., Schelvis, J. P. M., Brandish, P. E., Zhao, Y., Babcock, G. T., and Marletta, M. A. (2000) Interaction of soluble guanylate cyclase with YC-1: Kinetic and resonance Raman studies. *Biochemistry 39*, 4191−4198.
(59) Derbyshire, E. R., Fernhoff, N. B., Deng, S., and Marletta, M. A. (2009) Nucleotide regulation of soluble guanylate cyclase substrate specificity. *Biochemistry 48*, 7519−7524.
(60) Yoo, B. K., Lamarre, I., Martin, J. L., and Negrerie, M. (2012) Quaternary structure controls ligand dynamics in soluble guanylate cyclase. *J. Biol. Chem. 287*, 6851−6859.
(61) Friebe, A., and Koesling, D. (1998) Mechanism of YC-1-induced activation of soluble guanylate cyclase. *Mol. Pharmacol. 53*, 123−127.
(62) Baskaran, P., Heckler, E. J., van den Akker, F., and Beuve, A. (2011) Identification of residues in the heme domain of soluble guanylyl cyclase that are important for basal and stimulated catalytic activity. *PLoS One 6*, e26976.
(63) Baskaran, P., Heckler, E. J., van den Akker, F., and Beuve, A. (2011) Aspartate 102 in the heme domain of soluble guanylyl cyclase has a key role in NO activation. *Biochemistry 50*, 4291−4297.
(64) Underbakke, E. S., Iavarone, A. T., and Marletta, M. A. (2013) Higher-order interactions bridge the nitric oxide receptor and catalytic domains of soluble guanylate cyclase. *Proc. Natl. Acad. Sci. U.S.A. 110*, 6777−6782.
(65) Martin, E., Lee, Y. C., and Murad, F. (2001) YC-1 activation of human soluble guanylyl cyclase has both heme-dependent and heme-independent components. *Proc. Natl. Acad. Sci. U.S.A. 98*, 12938−12942.
(66) Martin, E., Sharina, I., Kots, A., and Murad, F. (2003) A constitutively activated mutant of human soluble guanylyl cyclase (sGC): Implication for the mechanism of sGC activation. *Proc. Natl. Acad. Sci. U.S.A. 100*, 9208−9213.
(67) Winger, J. A., and Marletta, M. A. (2005) Expression and characterization of the catalytic domains of soluble guanylate cyclase: Interaction with the heme domain. *Biochemistry 44*, 4083−4090.
(68) Russwurm, M., and Koesling, D. (2004) NO activation of guanylyl cyclase. *EMBO J. 23*, 4443−4450.
(69) Cary, S. P., Winger, J. A., and Marletta, M. A. (2005) Tonic and acute nitric oxide signaling through soluble guanylate cyclase is mediated by nonheme nitric oxide, ATP, and GTP. *Proc. Natl. Acad. Sci. U.S.A. 102*, 13064−13069.
(70) Tsai, A. L., Berka, V., Sharina, I., and Martin, E. (2011) Dynamic ligand exchange in soluble guanylyl cyclase (sGC): Implications for sGC regulation and desensitization. *J. Biol. Chem. 286*, 43182−43192.
(71) Tsai, A. L., Martin, E., Berka, V., and Olson, J. S. (2012) How do heme-protein sensors exclude oxygen? Lessons learned from cytochrome c′, *Nostoc puntiforme* heme nitric oxide/oxygen-binding domain, and soluble guanylyl cyclase. *Antioxid. Redox Signaling 17*, 1246−1263.
(72) Tsai, A. L., Berka, V., Martin, E., and Olson, J. S. (2012) A "sliding scale rule" for selectivity among NO, CO, and O_2 by heme protein sensors. *Biochemistry 51*, 172−186.
(73) Weichsel, A., Andersen, J. F., Roberts, S. A., and Montfort, W. R. (2000) Reversible nitric oxide binding to nitrophorin 4 from *Rhodnius prolixus* involves complete distal pocket burial. *Nat. Struct. Biol. 7*, 551−554.
(74) Kondrashov, D. A., and Montfort, W. R. (2007) Nonequilibrium dynamics simulations of nitric oxide release: Comparative study of nitrophorin and myoglobin. *J. Phys. Chem. B 111*, 9244−9252.
(75) Benabbas, A., Ye, X., Kubo, M., Zhang, Z., Maes, E. M., Montfort, W. R., and Champion, P. M. (2010) Ultrafast dynamics of diatomic ligand binding to nitrophorin 4. *J. Am. Chem. Soc. 132*, 2811−2820.
(76) Stone, J. R., and Marletta, M. A. (1995) The ferrous heme of soluble guanylate cyclase: Formation of hexacoordinate complexes with carbon monoxide and nitrosomethane. *Biochemistry 34*, 16397−16403.
(77) Martin, E., Berka, V., Bogatenkova, E., Murad, F., and Tsai, A. L. (2006) Ligand selectivity of soluble guanylyl cyclase: Effect of the hydrogen-bonding tyrosine in the distal heme pocket on binding of oxygen, nitric oxide, and carbon monoxide. *J. Biol. Chem. 281*, 27836−27845.